Volume 9 Issue 3 (2021) 249-254 ISSN 2347 - 3258
International Journal of Advance Research and Innovation

Optimization of Power and Efficiency in a segmented legs STEG using the Taguchi method

Princy Mishra, OP Singh, AK Katiyar
Department of Applied Science and Humanities, Institute of Engineering and Technology, Dr. A P J Abdul Kalam Technical University, Lucknow-226021, India.

Article Info
Article history:
Received 18 May 2021
Received in revised form
28 July 2021
Accepted 5 September 2021
Available online 15 September 2021

Keywords: Thermoelectric, optimization, segmented, power output, efficiency

Abstract: In the recent times, many researchers have concentrated on the development of thermoelectric materials with higher values of figure of merits to enhance the conversion efficiency. It have been observed in some of the previous studies that the figure of merit and hence, the performance of thermoelectric modules can be enhanced using the module with segmented legs of two or more thermoelectric materials. In this study, the application of segmented thermoelectric modules in a solar assisted thermoelectric generator have been presented. PbTe and BiTe alloys are used in the segmented module. Except the figure of merit, the performance of thermoelectric generator is also dependent on temperatures across modules, load resistance and various design parameters such as leg geometries, cross sectional area of legs etc. So, Taguchi method of optimization was employed using five factors and five levels design to optimize the power and conversion efficiency. The power and efficiencies are mathematically calculated at different combinations according to L25 orthogonal array. The maximum power output is predicted up to 31.52 W and conversion efficiency up to 14.61% using The Taguchi analysis. Analysis of Variance method is also used to analyze general linear model which results into the estimation of contribution percentages of each factor on the power and efficiency.

1. Introduction

TEGs) offer an exclusive solution for electrical energy generation by utilization of waste heat in various applications such as recovery of automobile exhaust waste heat, waste heat utilization in solar thermal applications etc. The working of thermoelectric module is based on 'Seebeck effect' and its operation is noise free and without any pollution [1]. So, TEGs can be used as a promising technology in waste heat utilization processes. But the usage of thermoelectric modules are still limited in converting low grade thermal energy into electricity. To overcome this limitation, there is a need to develop thermoelectric materials with higher values of figure of merit (ZT) than the existing values of ZT. The heat to electrical conversion efficiency of thermoelectric modules depends upon the temperatures of both sides across module (T_h and T_c) and figure of merit (ZT) [2].

$$\eta_{TEG} = \frac{\Delta T}{T_h} \cdot \frac{\left(\sqrt{(1+ZT)}-1\right)}{\left(\sqrt{(1+ZT)}+\frac{T_c}{T_h}\right)} \quad (1)$$

The theoretical efficiency of the TEG can be calculated using the equation (1). The dimensionless figure of merit (ZT) determines the performance of thermoelectric material. The ZT Values depend on various parameters such as electrical resistivity ρ, Seebeck coefficient α, Average of both side temperatures T and thermal conductivity k [2].

$$ZT = \frac{\alpha^2}{k.\rho}T \quad (2)$$

In the previous two decades, many researchers focused on the augmentation of the value of figure of merit (ZT) of thermoelectric materials. As it is depicted from equation (2), that ZT can be augmented by decreasing the thermal conductivity 'k' and by increasing the factor α^2/ρ. Also, the figure of merit is dependent on temperature. Higher values of ZT can be attained by employing TE materials at higher temperatures. Generally, bismuth-telluride (Bi-Te) alloys are normally used in the temperature range 100°C - 200°C [3-8]. At higher temperatures, skutterudites (300°C - 600°C) and Pb-Te alloys (350°C - 650°C) are used [9-13]. At very high temperature (range 900°C - 950°C), Si-Ge alloys can be employed in waste heat recovery applications [14-15]. Half-heusler alloys are also good option in the temperature range 500°C - 800°C [16-17].

Corresponding Author,
E-mail address: princess.mishra07@gmail.com, opsingh@ietlucknow.ac.in, akkatiyar@ietlucknow.ac.in

Some of the recent advancements in the TE materials are shown in the table 1.

Table 1: Enhanced ZT values of some newly developed TE material

Authors	TE Materials developed	Temp. Range	ZT value	Ref.
Xie et al.	p-type nanostructured $(Bi,Sb)_2Te_3$	300 – 450 K	1.4	[18]
Zhao et al.	p-type MgAgSb-based bulk material	475 K	1.4	[19]
Wu et al.	p-type K-doped $PbTe_{0.7}S_{0.3}$ bulk material	550 K – 800 K	1.56 – 2.2	[20]
Zhao et al.	p-type SnSe single crystals	923 K	2.6 ± 0.3	[21]
Liu et al.	BiTeSe bulk materials	300 K – 500 K	Little > 1.0	[22]
Hsu et al.	$AgPb_mSbTe_{2+m}$	800 K	2.2	[23]
Shi et al.	Multiple-filled skutterudites	850 K	1.7	[24]
Basu et al.	Silicon germanium alloys ($Si_{80}Ge_{20}$)	1073 K	1.84	[25]

Some of the recent studies are focused on the development of segmented thermoelectric modules by using combination of different materials. In case of segmented TE modules, two or more TE materials are linked in series which enable modules to operate in a greater temperature range and with comparatively higher ZT value than in case of non-segmented TE modules. In this work, the study and optimization analysis of solar assisted TEGs have been presented with the segmented legs of TE materials. The literature regarding segmented TEGs have been presented in next section. Firstly, the concept of solar assisted TEG is presented here.

As we know that solar energy is a viable source of renewable energy. Due to depletion of conventional source of energy, utilizing solar energy is a promising technique to deal with the problem of energy scarcity. Solar energy can be directly transformed into electrical energy by means of two technologies. First is the use of solar photovoltaic cells which alters photon energy into electricity through electron–hole pair generation. The other technology for direct solar to electrical conversion is the use of thermoelectric modules. Usually, an adequate amount of thermal energy is wasted in solar thermal application. This waste thermal energy can be utilized if we install thermoelectric modules in such a way that one side of modules is exposed to solar energy and the other side is exposed to air or water cooled heat sink. Due to this, a temperature

difference is created across TE modules and voltage induces on the basis of Seebeck effect. This type of thermoelectric generator can be named as solar assisted thermoelectric generator (STEG). STEG can be defined as a device which is used to harness waste heat of solar thermal applications and convert it into electrical energy. STEGs are environmental friendly, highly reliable devices having noise-free operation and long life. Moreover, a greater part of solar spectrum can be harnessed in case of STEGs [26-27].

2.Description of segmented STEGs

2.1 Literature review of segmented thermoelectric modules

A few researchers have proposed the used of segmented TEGs for greater performance. A compatibility function was recommended by Snyder et al. which illustrates the viability of linking two or more TE materials without any adverse effect [28-29]. Hadjistassou et al. proposed a method to design TEGs with segmented Bi_2Te_3-PbTe legs. In this work, a comparative analysis was done to compare the values of Seebeck coefficients of segmented TE module with the pure PbTe and Bi_2Te_3 materials [30]. Similarly, McEnaney et al. proposed a design model of segmented TEGs with Bi_2Te_3 and Skutterudite materials [31]. Ngan et al. presented a numerical model in which the theoretical efficiencies were calculated for various combinations of segmented TE modules [32]. Xiao et al. proposed a model with a pair of p-type and n-type elements with Bi_2Te_3 and filled- skutterudite [33]. Erturun et al. designed a 4-leg model with segmented materials BiTe and CoSb-based Skutterudite. In this work, the thermos-mechanical performance of the model was estimated [34]. Rezania et al. analyzed a model of p-type and n-type pair having various footprints. In this work, Authors studied the optimization of electrical energy generation using TE modules as p-type Zn_4Sb_3 and n-type $Mg_2Si_{1-x}Sn_x$ [35].

Hu et al. proposed a TEG module with segmented legs of Bi_2Te_3 and nanostructured PbTe. The results depicted that segmented TEG achieved the conversion efficiency of 11% at 590 K temperature difference while non-segmented nanostructured PbTe could achieve the efficiency up to 8.8% at temperature difference of 570 K [36].

Hadjistassou et al. presented the computational modeling of segmented Bi_2Te_3-PbTe TEG. A comparative analysis was performed for various designs of TEG. The results showed that the proposed system of segmented TEG could attain a maximum efficiency of 5.29% at the temperature difference of 325 K [37].

D'angelo et al. presented a system for the characterization of the conversion efficiency in case of segmented TE modules comprised of p-type $Bi_xSb_{2-x}Te_3$ to $Ag_{0.9}Pb_9Sn_9Sb_{0.6}Te_{20}$ legs and n-type $Bi_2Te_{3-x}Se_x$ to $Ag_{0.86}Pb_{19+x}SbTe_{20}$ legs. The results depicted that the maximum conversion efficiency was calculated as 6.56% for 400°C temperature at hot side and 23°C at the cold side [38].

2.2 Description of proposed system

The proposed system of solar assisted segmented TEG is shown in figure. In this system, Fresnel lenses are used to concentrate the solar irradiation on the solar absorbing surface at the hot side of TEG. A glass covering is used to enclose the TEG so that vacuum can be created and the effects from environmental factors can be minimized. A heat conducting surface is inserted between solar absorber and hot side of TEG surface. The thermal conductivity of heat conducting surface should be high. So, Copper or aluminum can be used. In this system, two thermoelectric materials (nanostructured PbTe and Bi_2Te_3) are linked to create segmented TEG. The performance of TEG can be augmented by use of segmented TEGs, as depicted in the literature review. An air or water cooled heat sink can be used at the cold side of TEG. The voltage difference induces due to temperature difference across TEG on the basis of Seebeck effect. The current flow through the load due to voltage difference created.

2.3 Process Parameters in the Solar assisted segmented TEG system

There are various parameters in solar assisted segmented TEG system such as intensity of solar radiation, hot side temperature of the TEG, cold side temperature of the TEG, figure of merit value of thermoelectric materials, thermal conductivity of interface material. Besides these parameters, the performance of segmented STEG system also depends upon design and arrangement of the TE modules such as height of different p-n legs, cross section area of p-n legs, resistive load, and gap between the different legs. The performance of TEG is also affected by the energy loss due to convection and radiation. Segmentation also increases thermal and electrical contact resistance at the interface of different legs which results in temperature drop at interface and generation of additional heat respectively.

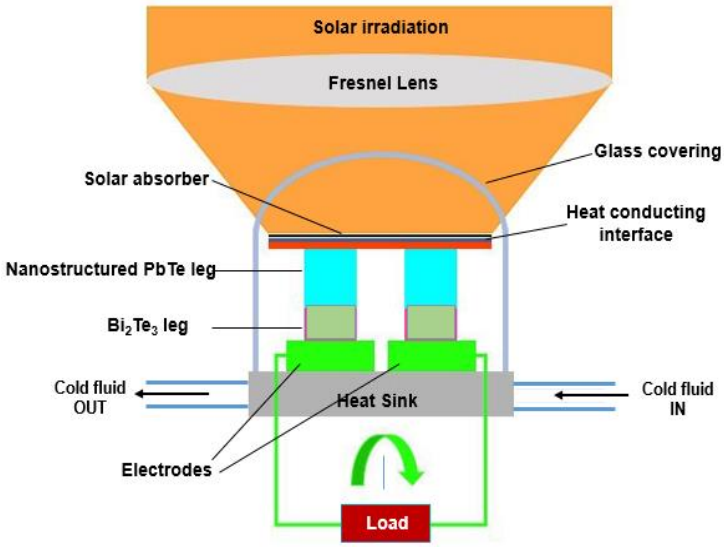

Fig. 1: Proposed system of segmented PbTe/BiTe legs STEG

3. Optimization of power and efficiency using taguchi method

In the previous section, it has been described that the performance of STEG is not only dependent on the figure of merit and temperatures across module but also on the leg geometries, cross sectional area and load resistance. Minitab software was used to optimize the power and efficiency of the STEG via Taguchi's approach. The steps in the Taguchi's approach are described in the subsequent sections:

3.1 Create Taguchi Design

In this optimization method, five factor and five levels design was selected in Taguchi method of optimization as shown in the table 2. An orthogonal array L25 was selected using the options available for 5-factor 5-level design. Thus, the number of runs were drastically reduced to 25 from 5^5 = 3125 runs in case of conventional optimization. The L25 orthogonal array is depicted in the table 3.

Table 2: Factors and their levels

Factors		Levels				
		(1)	**(2)**	**(3)**	**(4)**	**(5)**
A	Hot Side Temperature T_h (°C)	200	300	400	500	600
B	BiTe p-n leg height (mm)	1.25	1.5	1.75	2.0	2.25
C	PbTe p-n leg height (mm)	1.75	2.0	2.25	2.5	2.75
D	Cross-sectional area, A (mm^2)	1.5 × 1.5	1.75 × 1.75	2.0 × 2.0	2.25 × 2.25	2.5 × 2.5
E	Load Resistance (Ω)	1.0	2.0	3.0	4.0	5.0

Table 3: L25 Orthogonal Array

S. No.	A	B	C	D	E
1.	1	1	1	1	1
2.	1	2	2	2	2
3.	1	3	3	3	3
4.	1	4	4	4	4
5.	1	5	5	5	5
6.	2	1	2	3	4
7.	2	2	3	4	5
8.	2	3	4	5	1
9.	2	4	5	1	2
10.	2	5	1	2	3
11.	3	1	3	5	2
12.	3	2	4	1	3
13.	3	3	5	2	4
14.	3	4	1	3	5
15.	3	5	2	4	1
16.	4	1	4	2	5
17.	4	2	5	3	1
18.	4	3	1	4	2
19.	4	4	2	5	3
20.	4	5	3	1	4
21.	5	1	5	4	3
22.	5	2	1	5	4
23.	5	3	2	1	5
24.	5	4	3	2	1
25.	5	5	4	3	2

3.2 Power and efficiency calculation

Once, the Taguchi design is created, response columns are entered either after performing the experiments using combinations of factor values given in the L25 array or after simulation/mathematical analysis. In this work, the published data was used for the properties of BiTe and PbTe materials as described by Hu X. et al. [36]. In case of segmented thermoelectric modules, the power and efficiencies at various combination of factors values were calculated mathematically using the following formulae [37]:

$$P = \frac{\alpha^2}{2\rho}\frac{AN}{(\zeta+1)(1+2\varepsilon l_c/l)^2}(T_h - T_c)^2 \quad (3)$$

$$\eta = \left(\frac{T_h - T_c}{T_h}\right)\left((1+2\varepsilon l_c/l)^2\left[2 - \frac{1}{2}\left(\frac{T_h - T_c}{T_h}\right) + \left(\frac{4}{ZT_h}\right)\left(\frac{1+\zeta}{1+2\varepsilon l_c}\right)\right]\right) \quad (4)$$

Where, α = Seebeck Coefficient
ρ = Electrical resistivity of module-legs
A = Cross-section area of module-legs
N = Number of thermoelectric modules
$\zeta = \frac{2\rho_c}{\rho}$ and $\varepsilon = \frac{\lambda_c}{\lambda}$, here ρ_c and λ_c represent electrical and thermal resistivity of interface between PbTe and BiTe layers; while ρ and λ denote are electrical and thermal resistivity of TE Materials.
l_c = thickness of interface
l = length of TE module
T_h = hot side temperature
T_c = cold side temperature
Z = figure of merit (K^{-1})
It is obvious from equation (3) and (4) that power and conversion efficiency for segmented TE modules are also the function of length, cross section area, module resistance and interface resistance besides the temperature and figure of merit value. In this work, the cold side temperature was kept constant at 30°C and the effect of environmental factor on the conversion efficiency was neglected. Only the five factor (as shown in table 2) were varied to optimize the output power and conversion efficiency. The power and efficiencies were calculated for all the 25 combination according to orthogonal array as depicted in the table 4.

Table 4: Power and efficiency calculated at all combination of L25 array

A	B	C	D	E	Power, P (watts)	Efficiency η (%)
1	1	1	1	1	2.244	2.64
1	2	2	2	2	3.357	4.7
1	3	3	3	3	2.81	5.04
1	4	4	4	4	2.804	4.65
1	5	5	5	5	1.503	3.4
2	1	2	3	4	6.13	6.77
2	2	3	4	5	6.022	6.21
2	3	4	5	1	6.502	7.68
2	4	5	1	2	3.733	4.73
2	5	1	2	3	8.996	7.6
3	1	3	5	2	10.912	9.51
3	2	4	1	3	8.495	7.53
3	3	5	2	4	9.99	10.06
3	4	1	3	5	11.761	8.7
3	5	2	4	1	14.336	8.2
4	1	4	2	5	16.579	12.5
4	2	5	3	1	10.744	8.33
4	3	1	4	2	27.188	11.67
4	4	2	5	3	16.481	10.7
4	5	3	1	4	14.737	9.44
5	1	5	4	3	25.56	14.77
5	2	1	5	4	21.932	10.88
5	3	2	1	5	25.03	11.96
5	4	3	2	1	12.609	6.06
5	5	4	3	2	20.073	12.05

3.3 Analyze Taguchi Design

Once, the response columns for power and efficiency are estimated, Taguchi design can be analyzed using 'Stat>DOE>Analyze Taguchi Design' tabs. In this process, the software asks for the option regarding signal to noise ratio in which "larger is better" option was selected because we want large value of power output and efficiency as much as possible. When we analyzed the Taguchi design for mean values of power and efficiency, the following results were generated. Table 5 and table 6 shows the response table for means of power and efficiency respectively, in which rank of factors is depicted as per the significance of factor in deciding power and efficiency. In this case, factor A, i.e. hot side temperature is having rank one which implies that factor 'A' is the most significant factor. The main effect plots for power and efficiency are generated as shown in figure 2-3. These main effect plots describe the variation of power and efficiency with respect to different levels of all five factors.

Table 5: Response table for power output (Mean)

Level	A	B	C	D	E
1	2.544	12.285	14.424	10.848	9.287
2	6.277	10.110	13.067	10.306	13.053
3	11.099	14.304	9.418	10.304	12.468
4	17.146	9.478	10.891	15.182	11.119
5	21.041	11.929	10.306	11.466	12.179
Delta	18.497	4.826	5.006	4.878	3.766
Rank	1	4	2	3	5

Table 6: Response Table for Efficiency (Mean)

Level	A	B	C	D	E
1	0.04086	0.09238	0.08298	0.07260	0.06582
2	0.06598	0.07530	0.08466	0.08184	0.08532
3	0.08800	0.09282	0.07252	0.08178	0.09128
4	0.10528	0.06968	0.08882	0.09100	0.08360
5	0.11144	0.08138	0.08258	0.08434	0.08554
Delta	0.07058	0.02314	0.01630	0.01840	0.02546
Rank	1	3	5	4	2

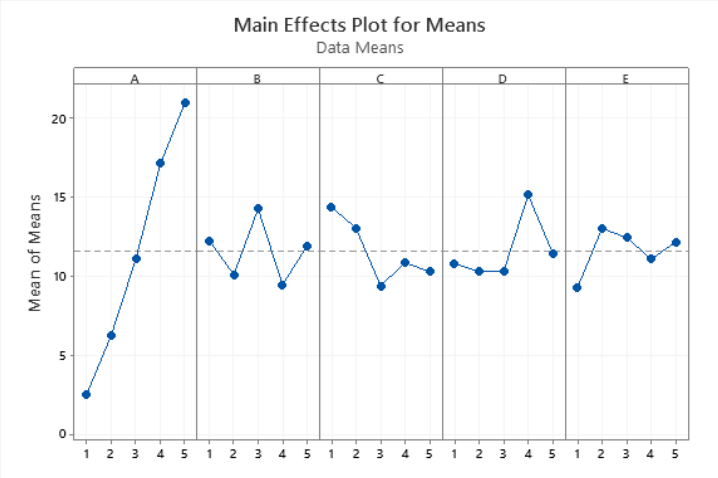

Fig. 2: Main effect plots for power output

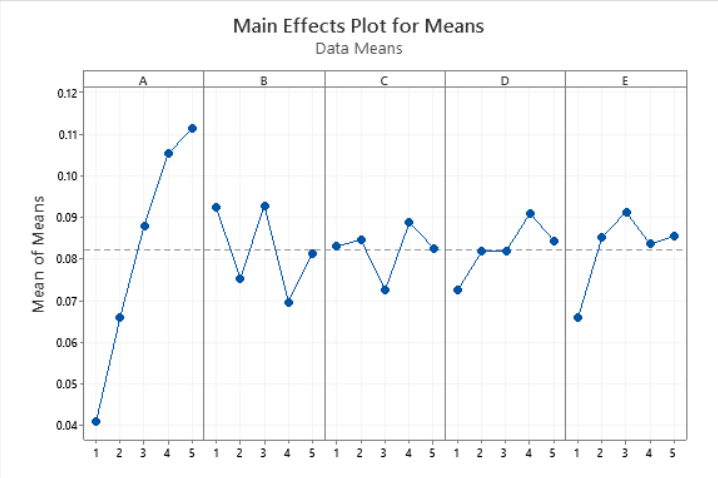

Fig. 3: Main effect plots for conversion efficiency

In this work, we have used five control factors for optimization but there exist a few noise factors too such as cold side ambient temperature of TE modules, environmental parameters such as heat lost due to convection and radiation, heat transfer coefficient etc. These noise factors are uncontrollable and can affect the performance of STEG system. In the Taguchi method, a 'Signal to Noise ratio (S/N ratio)' method is used to optimize the output after minimizing the losses. Taguchi method incorporates the use of loss function and changed it into the form of 'S/N ratios'. In the Taguchi optimization, there can be following types of S/N ratios on the basis of the optimization goal:

(a) Larger is better S/N ratios
(b) Smaller is better S/N ratios
(c) Nominal is best S/N ratios

In this work, we have used 'Larger is better S/N ratios' because we need the higher values of power and efficiency as much as possible. S/N ratio can be calculated using the equation (5) in case of 'larger is better option'. S/N ratio calculation is beneficial to estimate the deviation of the performance characteristic from the desired value. The larger value of S/N ratio results in the higher effect of control factors over noise factors on the output. Table 7 and 8 presents the response table for S/N ratios of power and efficiency respectively. Response tables show that hot side temperature is the most significant parameter for both power and efficiency determination. Also, load resistance and PbTe leg height are the least important parameter for power and efficiency respectively.

$$Larger\ is\ better \frac{S}{N}(dB) = -10log\left[\frac{1}{r}\sum_{i=1}^{r}\frac{1}{y_i^2}\right] \quad (5)$$

Here, 'r' – Number of data points & 'y_i' – Value of the i^{th} data point.

Table 7: Response Table for S/N Ratio of Power output

Level	A	B	C	D	E
1	7.802	19.214	20.604	17.676	17.809
2	15.625	18.428	20.341	19.199	19.492
3	20.774	20.377	18.142	18.562	19.826
4	24.282	17.632	18.849	20.904	18.977
5	26.202	19.034	16.749	18.344	18.581
Delta	18.400	2.745	3.855	3.227	2.016
Rank	1	4	2	3	5

Table 8: Response Table for S/N Ratio of efficiency

Larger is better

Level	A	B	C	D	E
1	-28.02	-22.01	-22.62	-23.90	-24.30
2	-23.74	-22.80	-21.91	-22.26	-22.11
3	-21.16	-21.06	-23.08	-22.10	-21.36
4	-19.64	-23.63	-21.57	-21.56	-21.95
5	-19.41	-22.47	-22.80	-22.16	-22.25
Delta	8.61	2.57	1.51	2.34	2.94
Rank	1	3	5	4	2

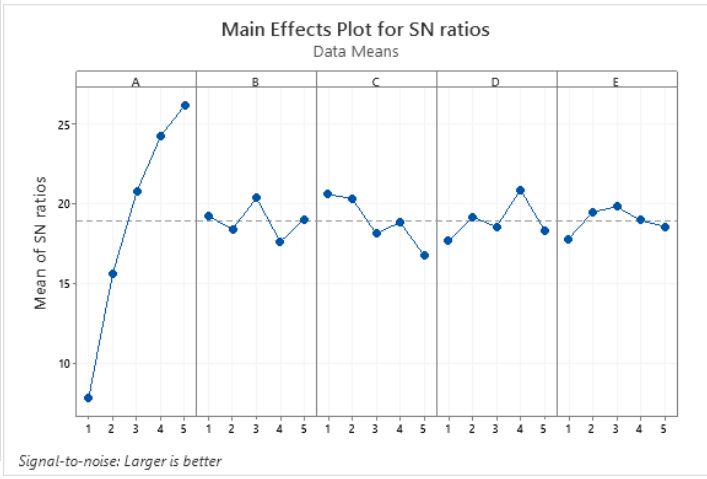

Fig. 4: Main effect plots for S/N Ratios of Power output

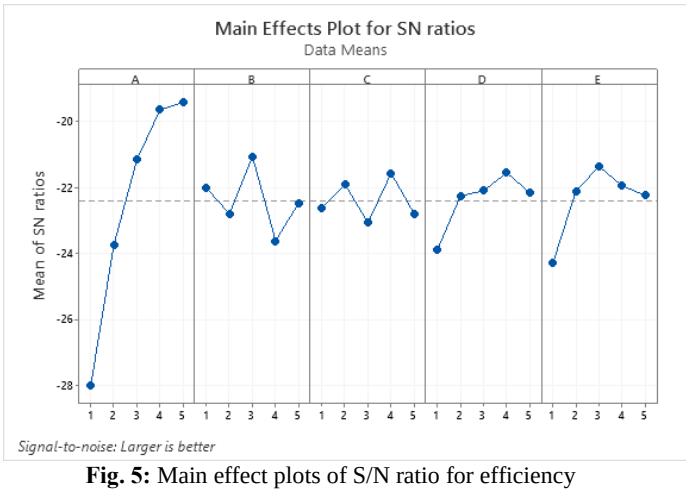

Fig. 5: Main effect plots of S/N ratio for efficiency

4. Determination of contribution of each factor in the power and efficiency estimation

The contribution of each factor in the power and efficiency estimation, can be determined using analysis of variance (ANOVA) technique in the Minitab software. For this purpose, 'Stat>ANOVA>General Linear Model' options are sequentially chosen to perform analysis of variance which results in the formation of ANOVA table. The contribution of each factor, degree of freedom, F-value and P-value are depicted by ANOVA table which is significant for the identification of most significant parameter. The contribution for each factor can be calculated using the following equation:

Table 9: ANOVA Table for Power Output (Variance Analysis)

Source	DF	Seq SS	Contribution	Adj SS	Adj MS	F-Value	P-Value
A	4	1152.45	79.76%	1152.45	288.113	180.43	0.000
B	4	73.06	5.06%	73.06	18.264	11.44	0.018
C	4	85.32	5.90%	85.32	21.330	13.36	0.014
D	4	83.83	5.80%	83.83	20.959	13.12	0.014
E	4	43.89	3.04%	43.89	10.974	6.87	0.044
Error	4	6.39	0.44%	6.39	1.597		
Total	24	1444.95	100.00%				

Table 10: ANOVA Table for Conversion Efficiency (Variance Analysis)

Source	DF	Seq SS	Contribution	Adj SS	Adj MS	F-Value	P-Value
A	4	0.016967	72.03%	0.016967	0.004242	16.64	0.009
B	4	0.002107	8.95%	0.002107	0.000527	2.07	0.250
C	4	0.000721	3.06%	0.000721	0.000180	0.71	0.627
D	4	0.000872	3.70%	0.000872	0.000218	0.86	0.558
E	4	0.001868	7.93%	0.001868	0.000467	1.83	0.286
Error	4	0.001019	4.33%	0.001019	0.000255		
Total	24	0.023554	100.00%				

4.1 Regression Equation

On the basis of analysis of variance method, regression equations are formed for power output and efficiency separately. These equations statistically generalize the formulae of power and efficiency for difference values of levels for different factors.

Regression Equation

Power, P = 11.621 - 9.078 A_1 - 5.345 A_2 - 0.522 A_3 + 5.525 A_4 + 9.420 A_5 + 0.664 B_1 - 1.511 B_2 + 2.683 B_3 - 2.144 B_4 + 0.308 B_5 + 2.803 C_1 + 1.446 C_2 - 2.203 C_3 - 0.731 C_4 - 1.315 C_5 - 0.773 D_1 - 1.315 D_2 - 1.318 D_3 + 3.561 D_4 - 0.155 D_5 - 2.334 E_1 + 1.431 E_2 + 0.847 E_3 - 0.503 E_4 + 0.558 E_5

Efficiency = 0.08231 - 0.04145 A_1 - 0.01633 A_2 + 0.00569 A_3 + 0.02297 A_4 + 0.02913 A_5 + 0.01007 B_1 - 0.00701 B_2 + 0.01051 B_3 - 0.01263 B_4 - 0.00093 B_5 + 0.00067 C_1 + 0.00235 C_2 - 0.00979 C_3 + 0.00651 C_4 + 0.00027 C_5 - 0.00971 D_1 - 0.00047 D_2 - 0.00053 D_3 + 0.00869 D_4 + 0.00203 D_5 - 0.01649 E_1 + 0.00301 E_2 + 0.00897 E_3 + 0.00129 E_4 + 0.00323 E_5

4.2 Analysis of Results

On the basis of the Taguchi optimization method, it can be stated that the value of T_h (hot side temperature) is the most significant factor and power and efficiency values can be predicted after optimization using the following formula:

$$Y_{predicted} = \overline{X} + \sum_{i=1}^{m} (\overline{X_i} - \overline{X}) \quad (6)$$

Where $\overline{X_i}$ symbolizes the mean of the output results at the optimal level of factor i, $\overline{X}$ denotes the grand mean of all the output data, and 'm' represents the total number of control factors.

The predicted highest values of power was calculated as 30.16 W and conversion efficiency as 14.61%. The confirmation run conducted at $A_5B_3C_1D_4E_2$ provides the value of power output as 31.52 W which is 4.51% more than the predicted value. However, the optimized value of conversion efficiency was calculated as 14.61% at combination $A_5B_3C_4D_4E_3$ which is same as the predicted value.

On the basis of the ANOVA method, following contribution percentage were estimated:

Table 11: Contribution of various factors in deciding Power output

Control Factors		Contribution percentage
A	Hot Side Temperature T_h (°C)	79.76%
B	BiTe p-n leg height (mm)	5.06%
C	PbTe p-n leg height (mm)	5.90%
D	Cross-sectional area, A (mm^2)	5.80%
E	Load Resistance (Ω)	3.04%

Table 12: Contribution of various factors in deciding Conversion efficiency

Control Factors		Contribution percentage
A	Hot Side Temperature T_h (°C)	72.03%
B	BiTe p-n leg height (mm)	8.95%
C	PbTe p-n leg height (mm)	3.06%
D	Cross-sectional area, A (mm^2)	3.70%
E	Load Resistance (Ω)	7.93%

5. Conclusions

An overview of segmented thermoelectric generators was presented with the segmented legs of PbTe and BiTe alloys. As our aim is to attain the higher value of power output and conversion efficiency. So, the Taguchi method and analysis of variance (ANOVA) method were used to optimize the power and efficiency for a five factor and five level design. The maximum power output was achieved as 31.52 W at $A_5B_3C_1D_4E_2$ combination, i.e. at 600°C hot side temperature, 1.75 mm BiTe leg height, 1.75 mm PbTe leg height, 2.25 × 2.25 mm^2 cross sectional area and 2.0 Ω resistance load. Also, the maximum value of conversion efficiency was found 14.61% at $A_5B_3C_4D_4E_3$ combination, i.e. at 600°C hot side temperature, 1.75 mm BiTe leg height, 2.5 mm PbTe leg height, 2.25 × 2.25 mm^2 cross sectional area and 3.0 Ω resistance load.

ANOVA table were also generated to determine the significance of all the five control factors on the power and efficiency. Both power and efficiency are mostly affected by the hot side temperature among all the factors. So, the installation of solar concentrator should be done in such a way that the hot side temperature value maximize the performance of the system. However, the heights of PbTe and BiTe legs are also important factor and Thermal and electrical resistance of the interface should be minimized while employing the segmented TE modules. These segmented can withstand the higher range of temperature and have higher value of figure of merit. But the design optimization and manufacturing techniques of segmented TE modules are much complex. So future research must focus on the design and development of segmented TEGs and solar thermal energy can be effectively transformed into electrical energy by means of segmented TEGs, if it used in a cogeneration system. As the efficiency of alone TEG system is limited, cogeneration systems can be recommended to use TEG as auxiliary source of power in solar thermal applications.

Acknowledgement and Data Availability

The data that supports the findings of this study are available within the article. Also, the data related to optimization of power and efficiency have been generated using Taguchi's Method in the Minitab software.

References

[1]. I Basel, WH Ahmed. Thermoelectric Power Generation Using Waste-Heat Energy as an Alternative Green Technology, Recent Patents on Electrical Engineering, 2(1), 2009, 27-39.

[2]. R Mesalam, HR Williams, RM Ambrosi, J García-Cañadas, K Stephenson. Towards a comprehensive model for characterizing and assessing thermoelectric modules by impedance spectroscopy, Appl. Energy 226, 2018, 1208–1218.

[3]. X Yan, et al. Experimental studies on anisotropic thermoelectric properties and structures of n-type $Bi_2Te_{2.7}Se_{0.3}$. Nano letters 10, 2010, 3373–3378.

[4]. Y Cao, X Zhao, T Zhu, X Zhang, J Tu. Syntheses and thermoelectric properties of Bi_2Te_3/Sb_2Te_3 bulk nanocomposites with laminated nanostructure. Applied Physics Letters 92, 2008, 143106.
[5]. W Xie, X Tang, Y Yan, Q Zhang, TM Tritt. Unique nanostructures and enhanced thermoelectric performance of melt-spun BiSbTe alloys. Applied Physics Letters 94, 2009, 102-111.
[6]. W Xie, et al. Identifying the specific nanostructures responsible for the high thermoelectric performance of $(Bi,Sb)_2Te_3$ nanocomposites. Nano letters 10, 2010, 3283–3289.
[7]. Fan, S. et al. p-type $Bi_{0.4}Sb_{1.6}Te_3$ nanocomposites with enhanced figure of merit. Applied Physics Letters 96, 2010, 182104.
[8]. KT Kim, GH Ha. Fabrication and enhanced thermoelectric properties of alumina nanoparticle-dispersed $Bi_{0.5}Sb_{1.5}Te_3$ matrix composites. Journal of Nanomaterials 8, 2013.
[9]. JP Heremans et al. Enhancement of thermoelectric efficiency in PbTe by distortion of the electronic density of states. Science 321, 2008, 554–557.
[10]. KF Hsu et al. Cubic $AgPb_mSbTe_{2+m}$: bulk thermoelectric materials with high figure of merit. Science 303, 2004, 818–821.
[11]. PF Poudeu et al. Nanostructures versus Solid Solutions: Low Lattice Thermal Conductivity and Enhanced Thermoelectric Figure of Merit in $Pb_{9.6}Sb_{0.2}Te_{10-x}Se_x$ Bulk Materials. Journal of the American Chemical Society 128, 2006, 14347–14355.
[12]. Biswas, K. et al. High-performance bulk thermoelectrics with all-scale hierarchical architectures. Nature 489, 2012, 414–418.
[13]. G Rogl et al. Multifilled nanocrystalline p-type didymium–Skutterudites with ZT > 1.2. Intermetallics 18, 2010, 2435–2444.
[14]. G Joshi et al. Enhanced thermoelectric figure-of-merit in nanostructured p-type silicon germanium bulk alloys. Nano letters 8, 2008, 2008, 4670–4674.
[15]. X Wang et al. Enhanced thermoelectric figure of merit in nanostructured n-type silicon germanium bulk alloy. Applied Physics Letters 93, 2008, 193121.
[16]. G Joshi, et al. Enhancement of thermoelectric figure-of-merit at low temperatures by titanium substitution for hafnium in n-type half-Heuslers $Hf_{0.75-x}Ti_x$ $Zr_{0.25}NiSn_{0.99}Sb_{0.01}$. Nano Energy 2, 2013, 82–87.
[17]. X Yan, et al. Stronger phonon scattering by larger differences in atomic mass and size in p-type half-Heuslers $Hf_{1-x}Ti_xCoSb_{0.8}Sn_{0.2}$. Energy & Environmental Science 5, 2012, 7543–7548.
[18]. W Xie, et al. Identifying the specific nanostructures responsible for the high thermoelectric performance of (Bi, $Sb)_2Te_3$ nanocomposites. Nano Lett. 10, 2010, 3283–3289.
[19]. H Zhao et al. High thermoelectric performance of MgAgSb-based materials. Nano Energ. 7, 2014, 97–103.
[20]. Wu, H. et al. Broad temperature plateau for thermoelectric figure of merit ZT > 2 in phase-separated $PbTe_{0.7}S_{0.3}$. Nature Comm. 5, 2014, 4515.
[21]. Zhao, L.-D. et al. Ultralow thermal conductivity and high thermoelectric figure of merit in SnSe crystals. Nature 508, 2014, 373–377.
[22]. Liu, W. S. et al. Thermoelectric Property Studies on Cu-Doped n-type $Cu_xBi_2Te_{2.7}Se_{0.3}$ Nanocomposites. Adv. Energy Mater. 1, 2011, 577–587.
[23]. Hsu, K. F. et al. Cubic $AgPb_mSbTe_{2+m}$: bulk thermoelectric materials with high figure of merit. Science 303, 2004, 818–821.
[24]. Shi, X. et al. Multiple-filled skutterudites: high thermoelectric figure of merit through separately optimizing electrical and thermal transports. J. Am. Chem. Soc. 133, 2011, 7837–7846.
[25]. Basu, R. et al. Improved thermoelectric performance of hot pressed nanostructured n-type SiGe bulk alloys. J. Mater. Chem. A 2, 2014, 6922–6930.
[26]. R. Amatya, R.J. Ram: Solar Thermoelectric Generator for Micro-power Applications, Journal of Electronic Materials, 39(9), 2010.
[27]. D Kraemer, Q Jie, K McEnaney, F Cao, W Liu, LA Weinstein, J Loomis, Z Ren, G Chen: Nature Energy 1, 2016, 16153.
[28]. GJ Snyder, TS Ursell. Thermoelectric efficiency and compatibility. Phys. Rev. Lett. 91, 2003,148301.
[29]. GJ Snyder. Application of the compatibility factor to the design of segmented and cascaded thermoelectric generators. Appl. Phys. Lett. 84, 2004, 2436–2438.
[30]. C Hadjistassou, E Kyriakides, J Georgiou. Designing high efficiency segmented thermoelectric generators. Energ. Convers. Manage. 66, 2013, 165–172.
[31]. K McEnaney, D Kraemer, Z Ren, G Chen. Modeling of concentrating solar thermoelectric generators. J. Appl. Phys. 110, 2011, 074502.
[32]. PH Ngan et al. Towards high efficiency segmented thermoelectric unicouples. Phys. Status Solidi A 211, 2014, 9–17.
[33]. J Xiao, T Yang, P Li, P Zhai, Q Zhang. Thermal design and management for performance optimization of solar thermoelectric generator. Appl. Energ. 93, 2012, 33–38.
[34]. U Erturun, K Erermis, K Mossi. Effect of various leg geometries on thermo-mechanical and power generation performance of thermoelectric devices. Appl. Therm. Eng. 73, 2014, 126–139.
[35]. A Rezania, L Rosendahl, H Yin. Parametric optimization of thermoelectric elements footprint for maximum power generation. J. of Power Sources 255, 2014, 151–156.
[36]. X Hu. et al. Power generation from nanostructured PbTe-based thermoelectrics: comprehensive development from materials to modules. Energy & Environmental Science 9, 2016, 517–529.
[37]. C Hadjistassou, E Kyriakides, J Georgiou. Designing high efficiency segmented thermoelectric generators. Energy conversion and management 66, 2013, 165–172.
[38]. J D'Angelo et al. Electrical, thermal, and mechanical characterization of novel segmented-leg thermoelectric modules. Journal of electronic materials 40, 2011, 2051–2062.
[39]. D Rowe, G Min. Design theory of thermoelectric modules for electrical power generation. IEEE Proceedings-Science, Measurement and Technology 143, 1996, 351–356.